SUPPORTING MATERIAL

Bacteria-Driven Fossil Ecosystems as Paleoindicators of Active Continental Margins and the Role of Carbonate Sediment-Hosted Vents in Geodynamic Reconstructions

László Bujtor [1], Ildikó Gyollai [2,3], Máté Szabó [2,3], Ivett Kovács [2,3] and Márta Polgári [1,2,3,*]

[1] IInstitute of Geography and Environmental Sciences, Eszterházy Károly Catholic University, 6-8 Leányka Street, H-3300 Eger, Hungary; bujtor.laszlo@uni-eszterhazy.hu

[2] HUN-REN Research Centre for Astronomy and Earth Sciences, Institute for Geological and Geochemical Research, Budaörsi út 45, H-1112 Budapest, Hungary; gyollai.ildiko@csfk.org (I.G.); szabo.mate@csfk.org (M.S.); kovacs.ivett@csfk.org (I.K.)

[3] HUN-REN Research Centre for Astronomy and Earth Sciences, MTA Centre of Excellence, Konkoly Thege Miklós út 15-17, H-1121 Budapest, Hungary

[*] Correspondence: rodokrozit@gmail.com

Content

SI Figure S1 Samples and thin sections of samples

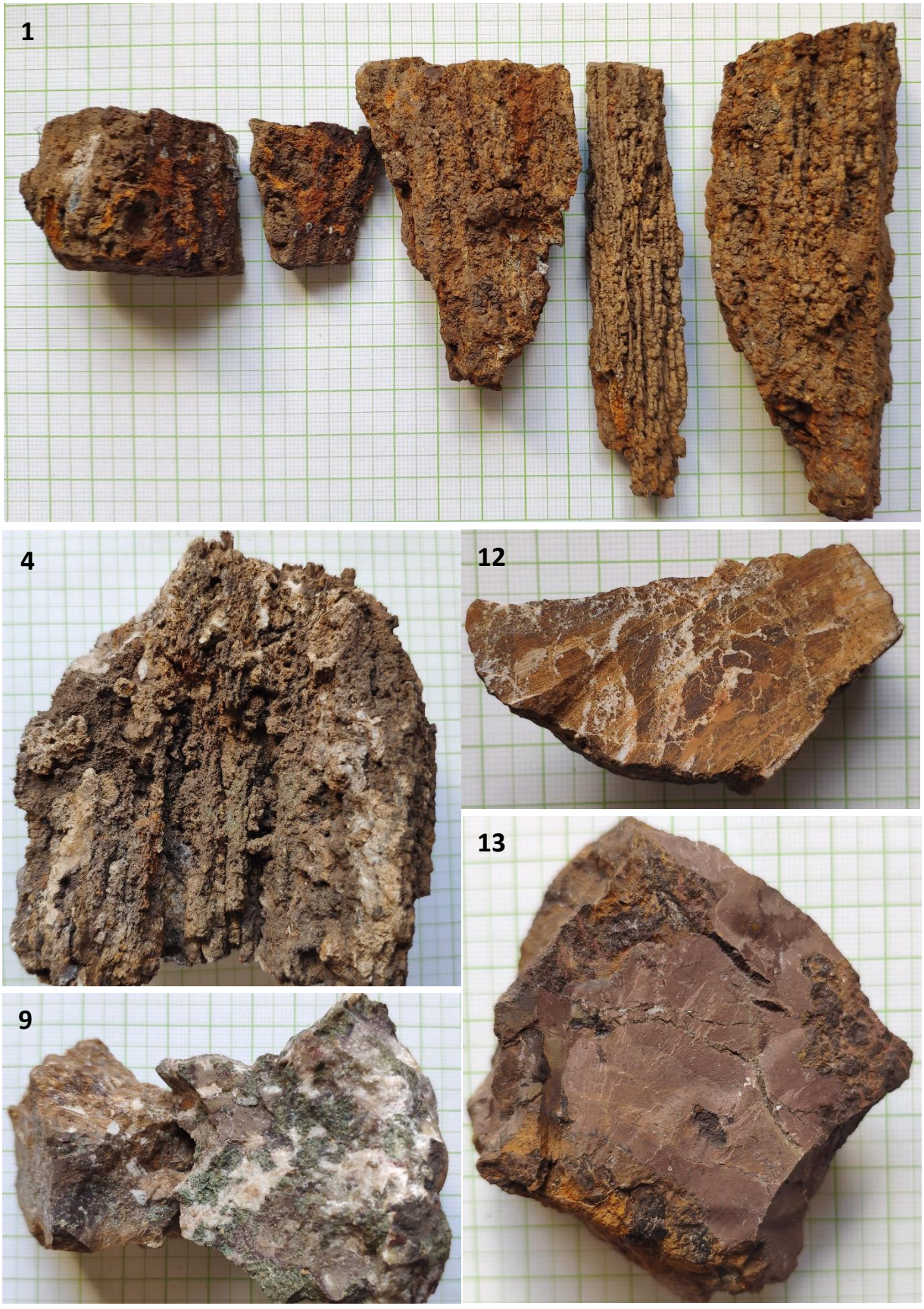

Scale: 1 cm

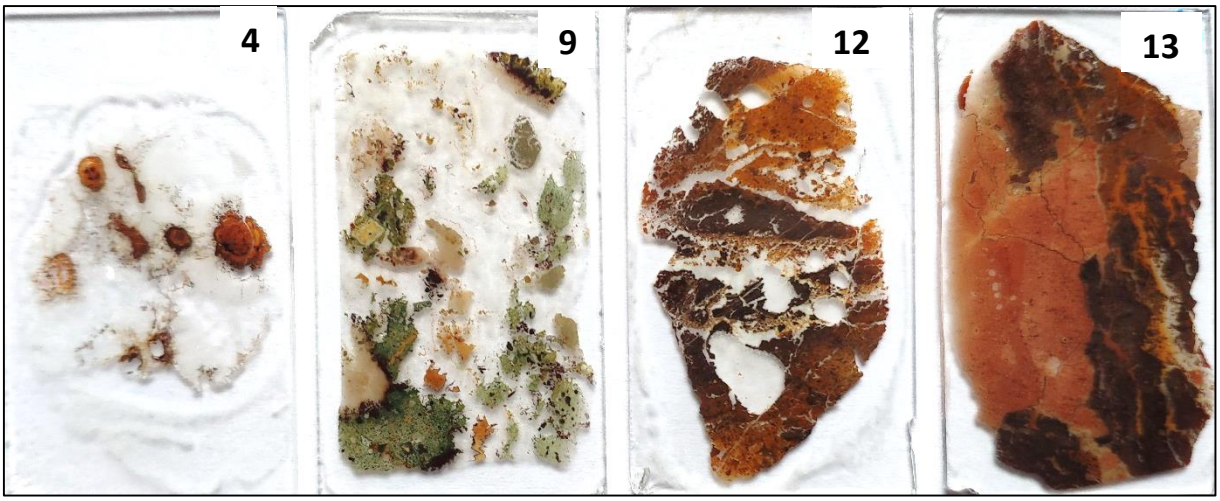
4
9
12
13


1

SI Figure S2 Optical rock microscopy photos

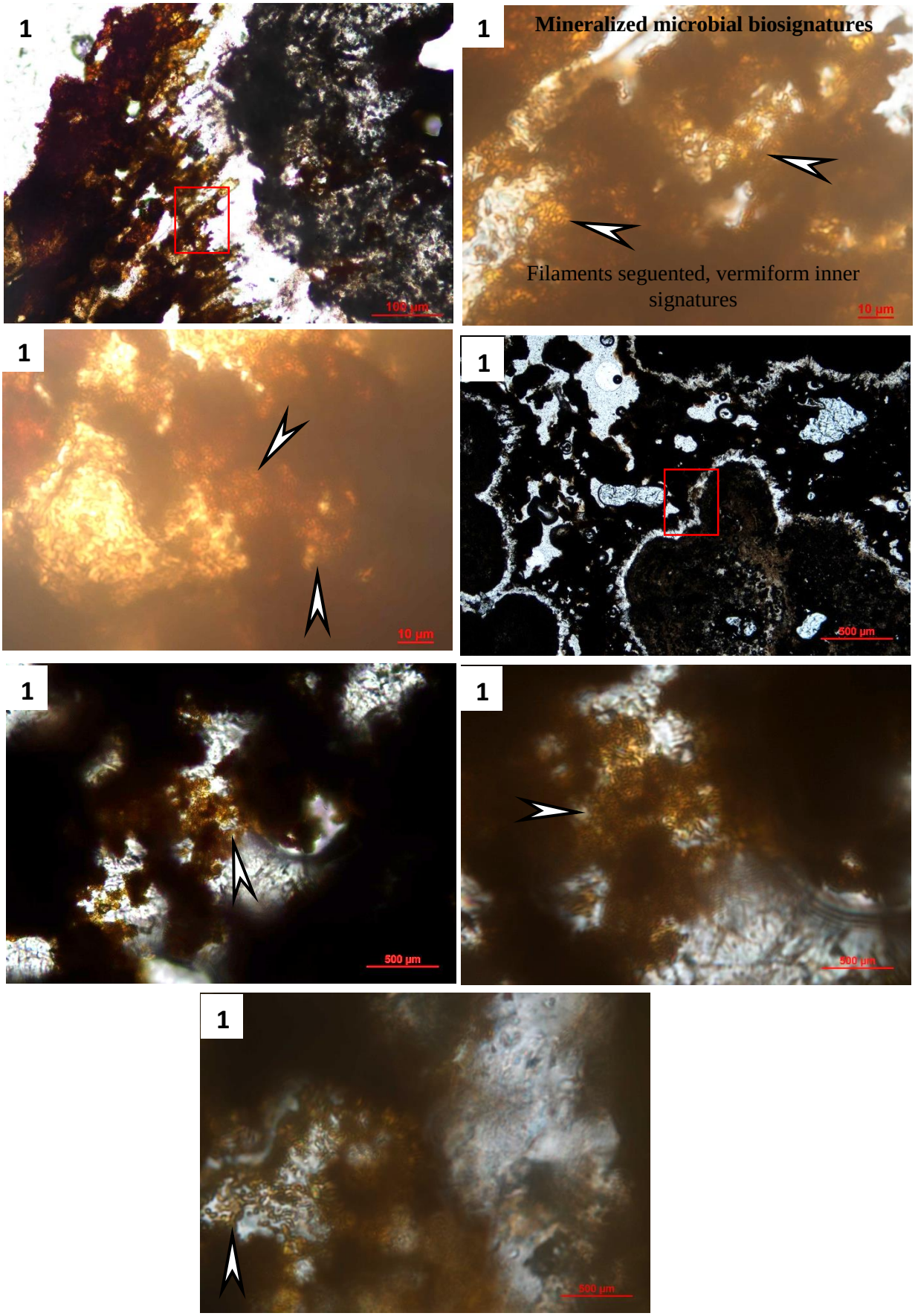

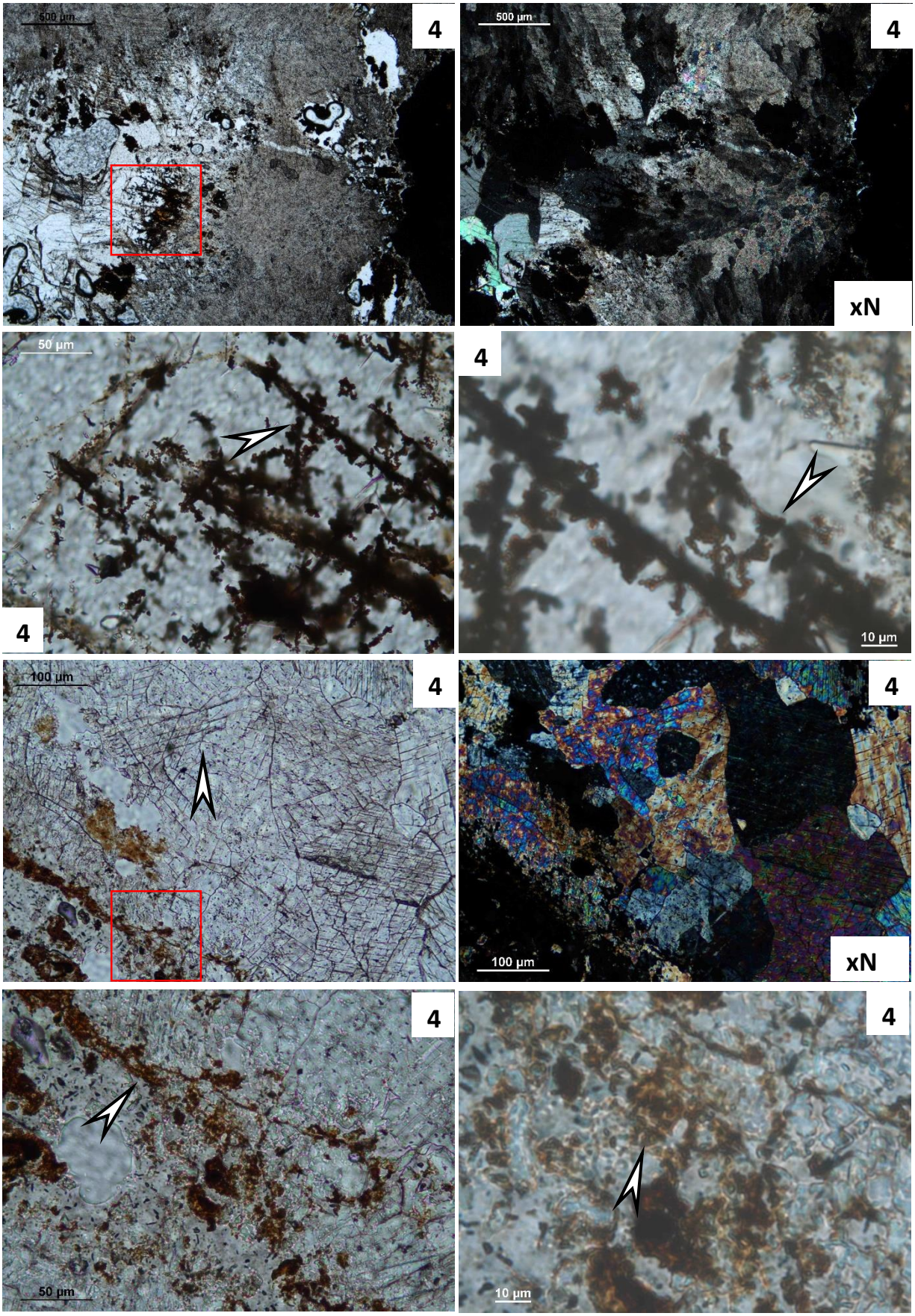
500 µm
4
500 µm
4
xN
50 µm
4
4
10 µm
100 µm
4
4
100 µm
xN
4
50 µm
4
10 µm

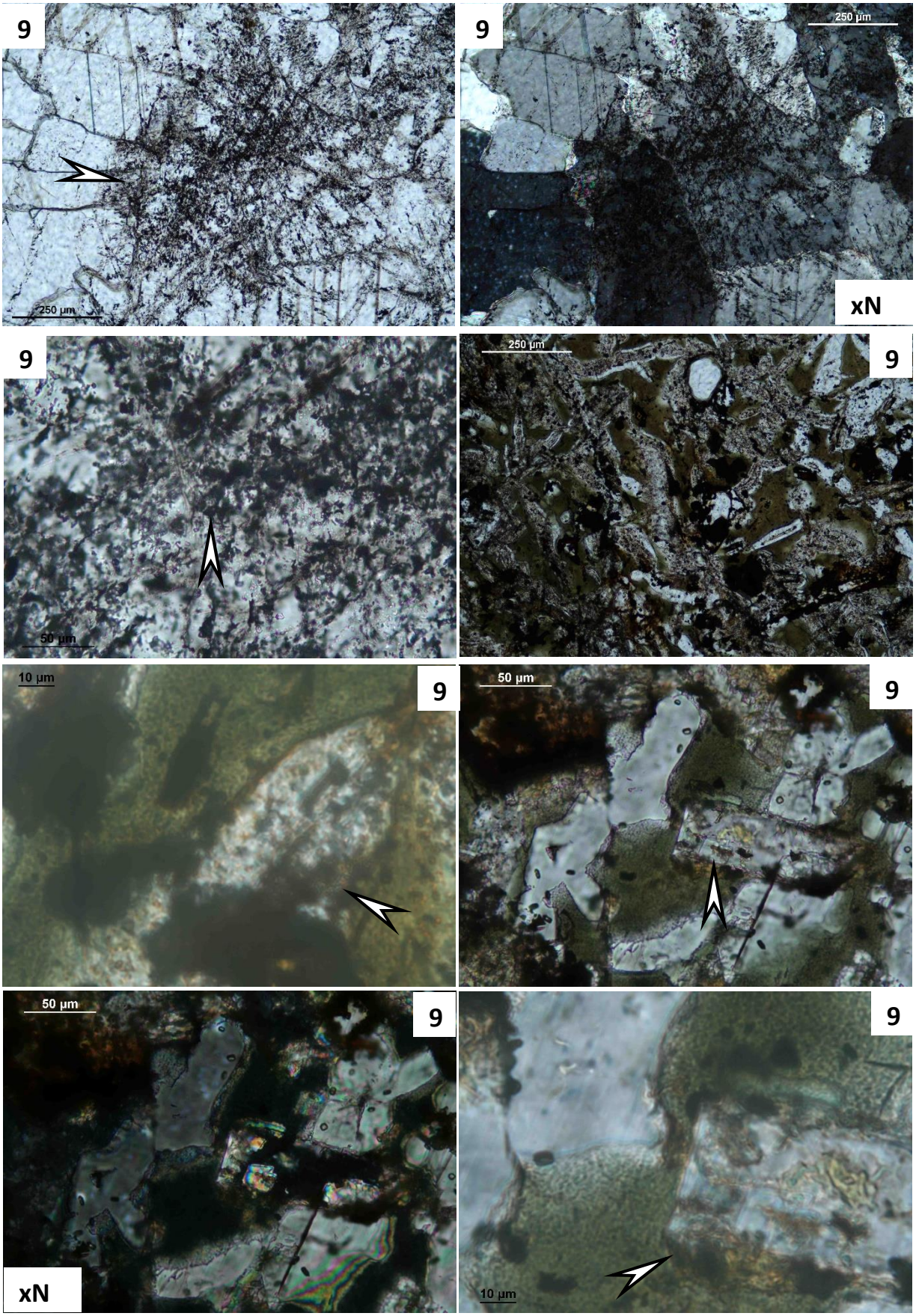
9
250 µm
9
250 µm
xN
9
50 µm
250 µm
9
10 µm
9
50 µm
9
50 µm
9
xN
9
10 µm

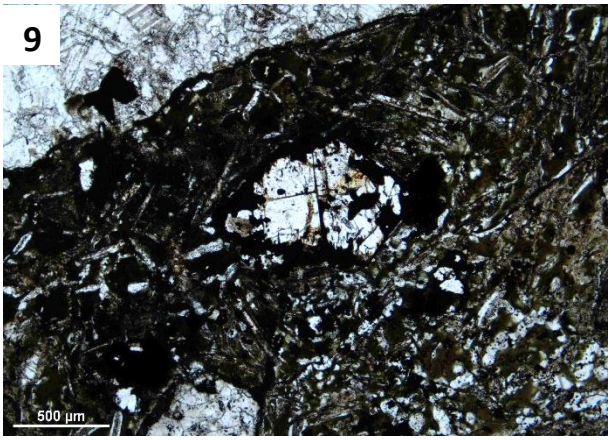
9
500 µm

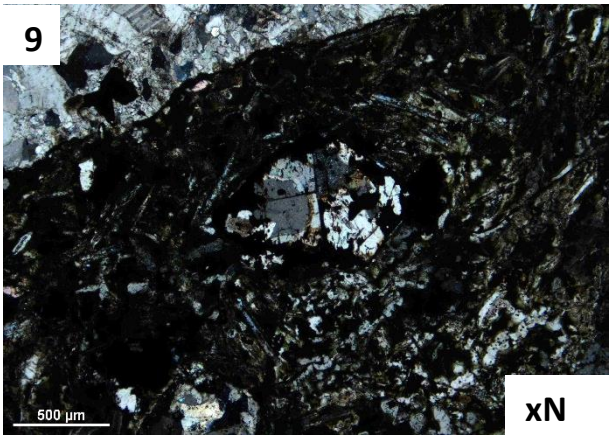
9
500 µm
xN

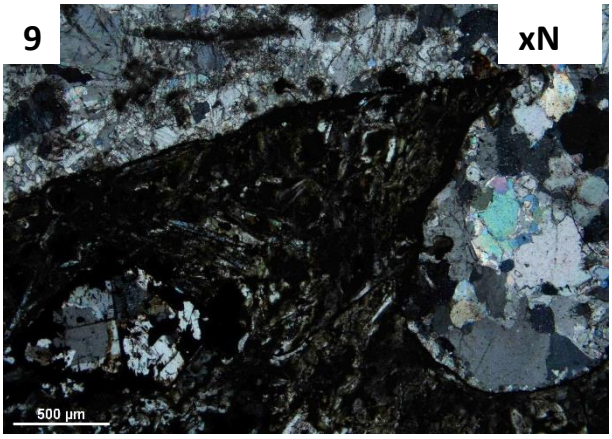
9
xN
500 µm

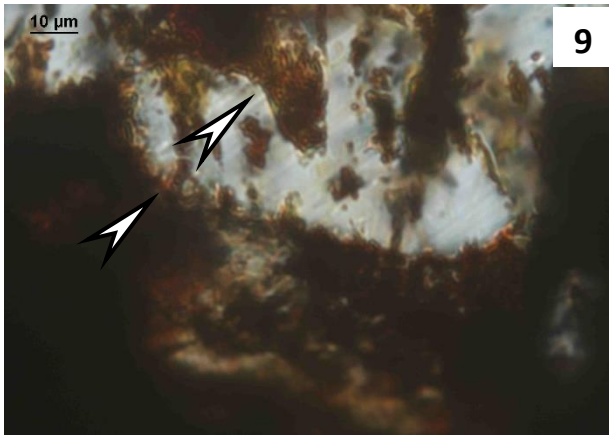
10 µm
9

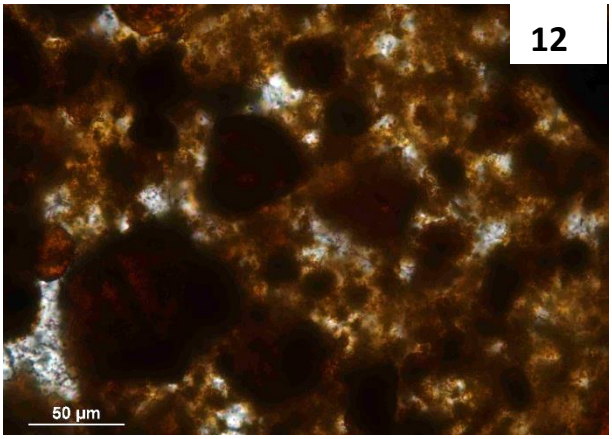
12
50 µm

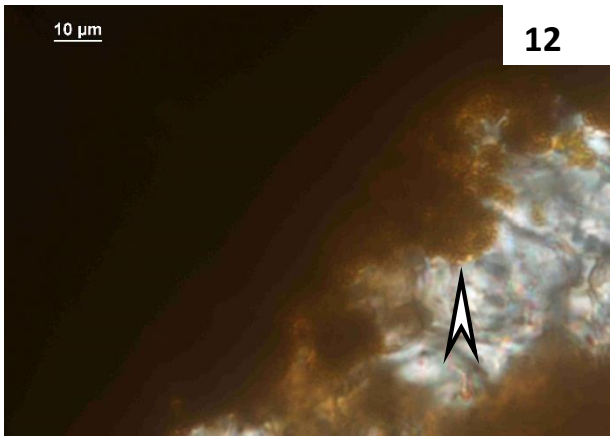
10 µm
12

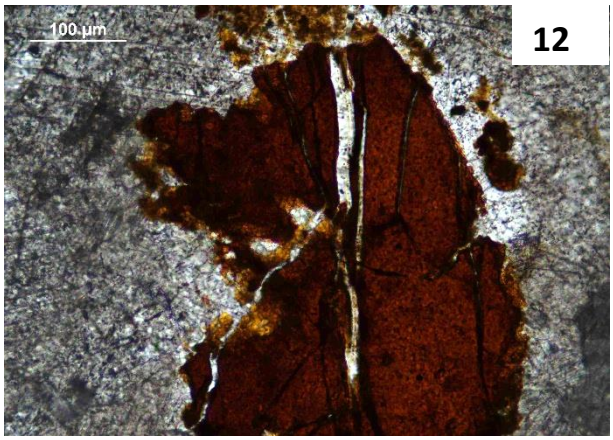
100 µm
12

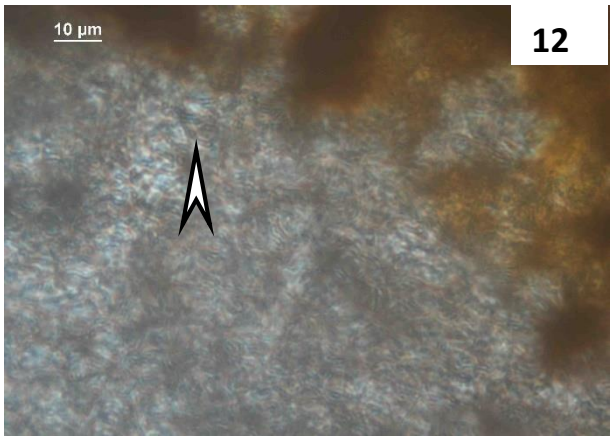
10 µm
12

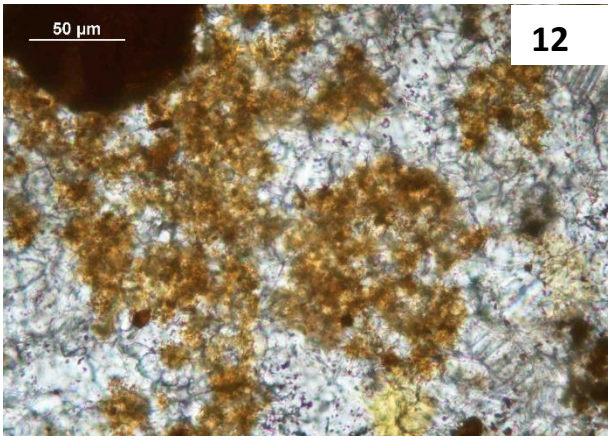
50 µm
12

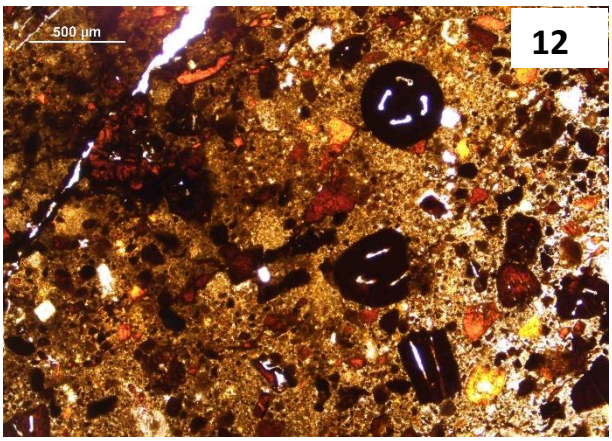
500 µm
12


100 µm
12

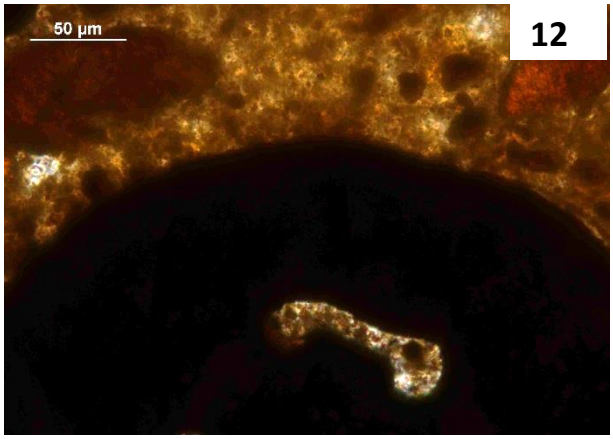
50 µm
12

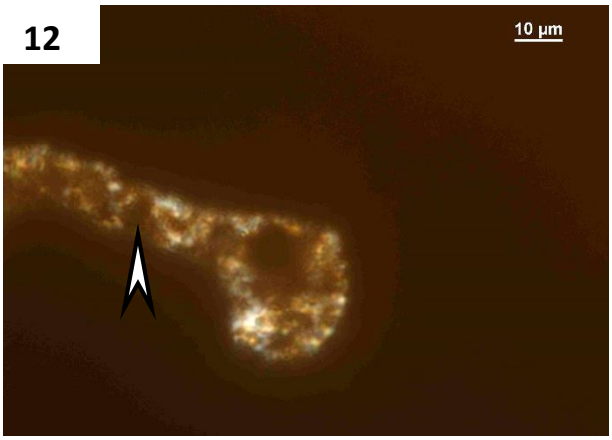
12
10 µm

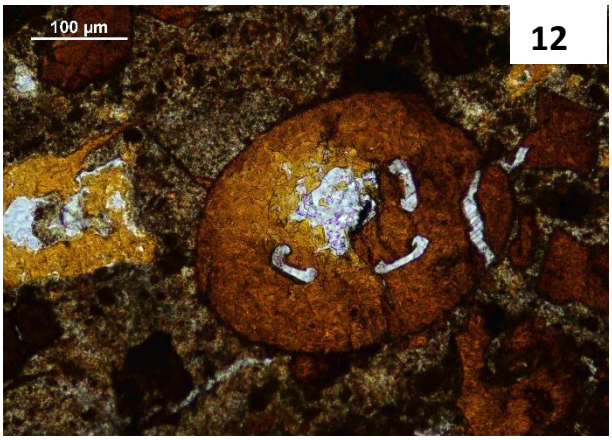
100 µm
12

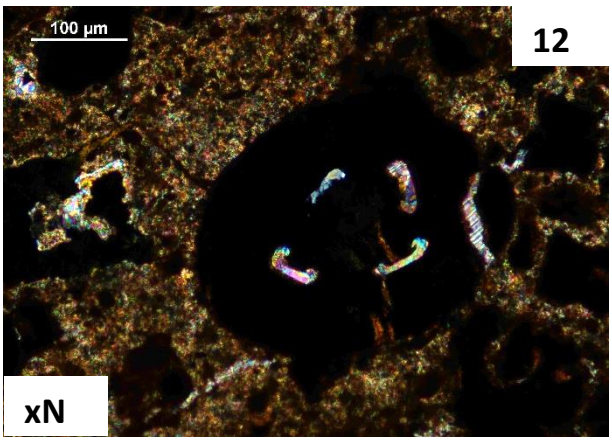
100 µm
12
xN


50 µm
12

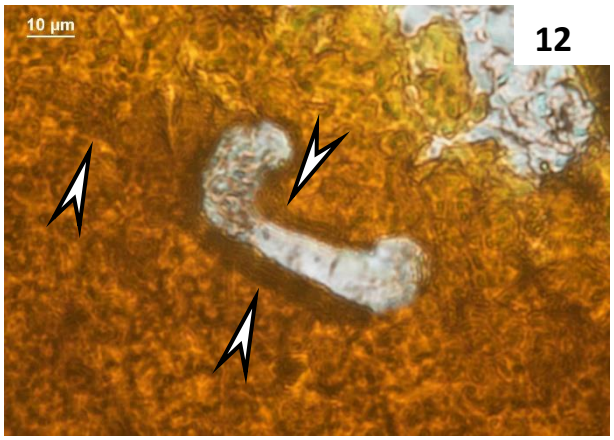
10 µm
12

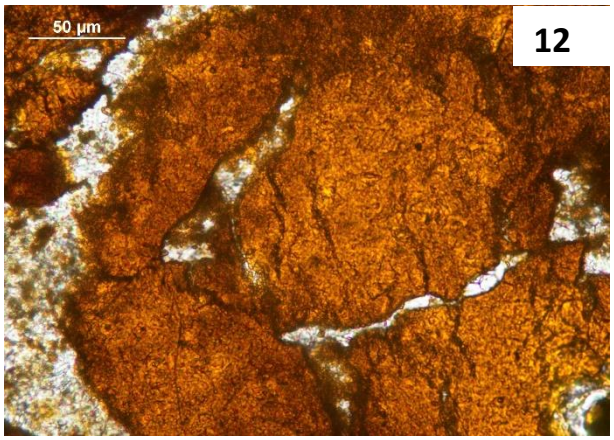
50 µm
12

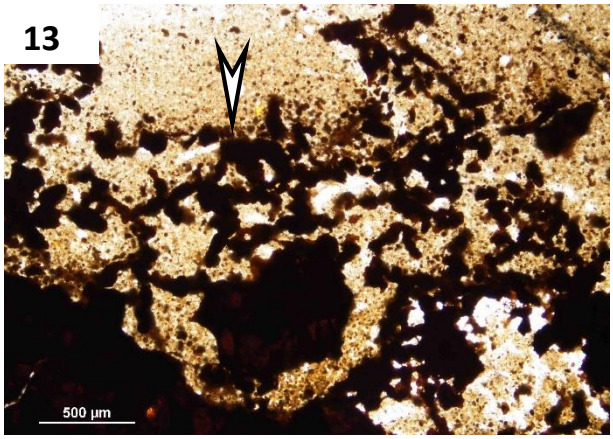
13
500 µm

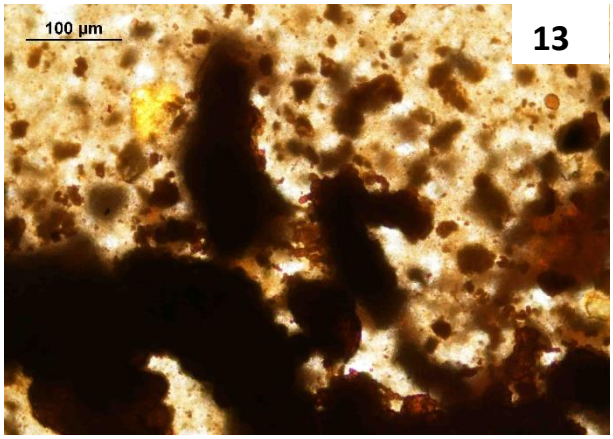
100 µm
13

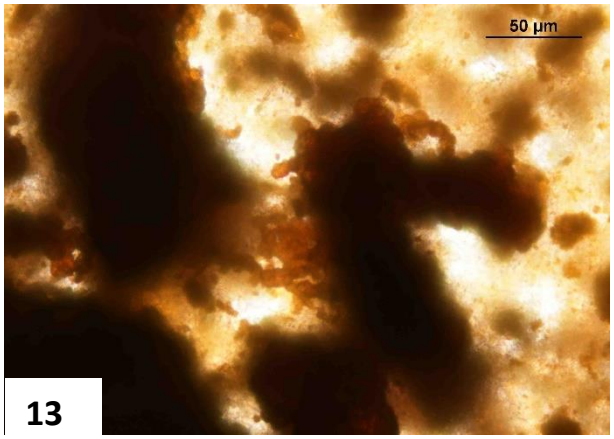
50 µm
13

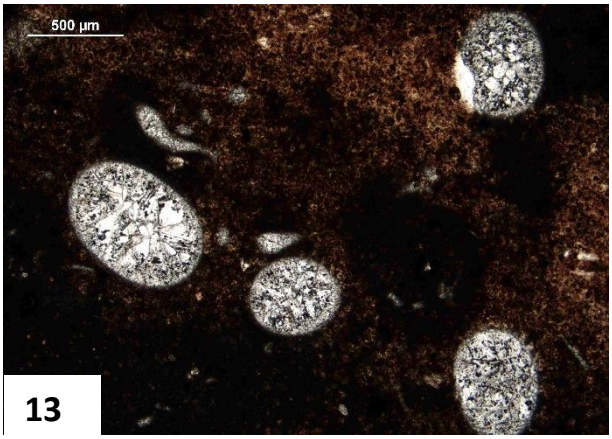
500 µm
13

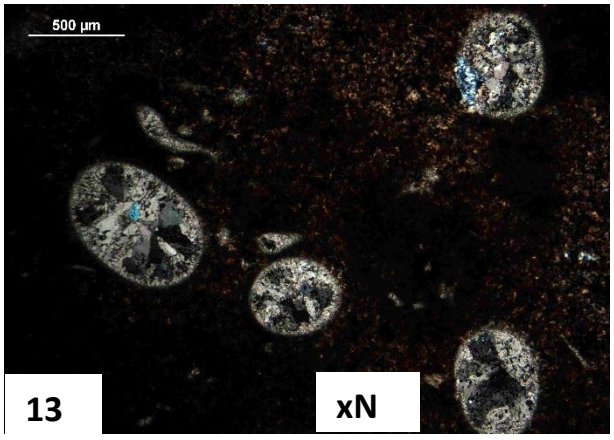
500 µm
13
xN

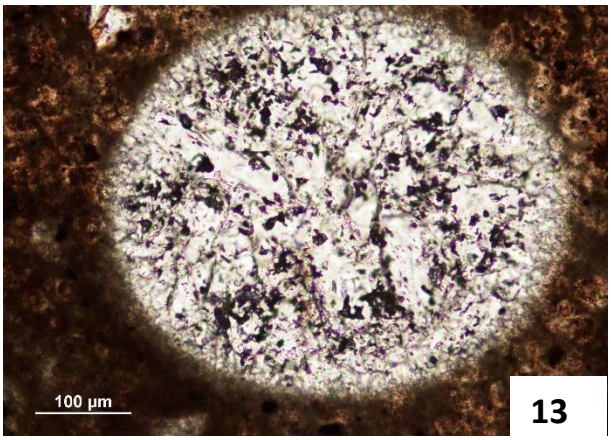
100 µm
13

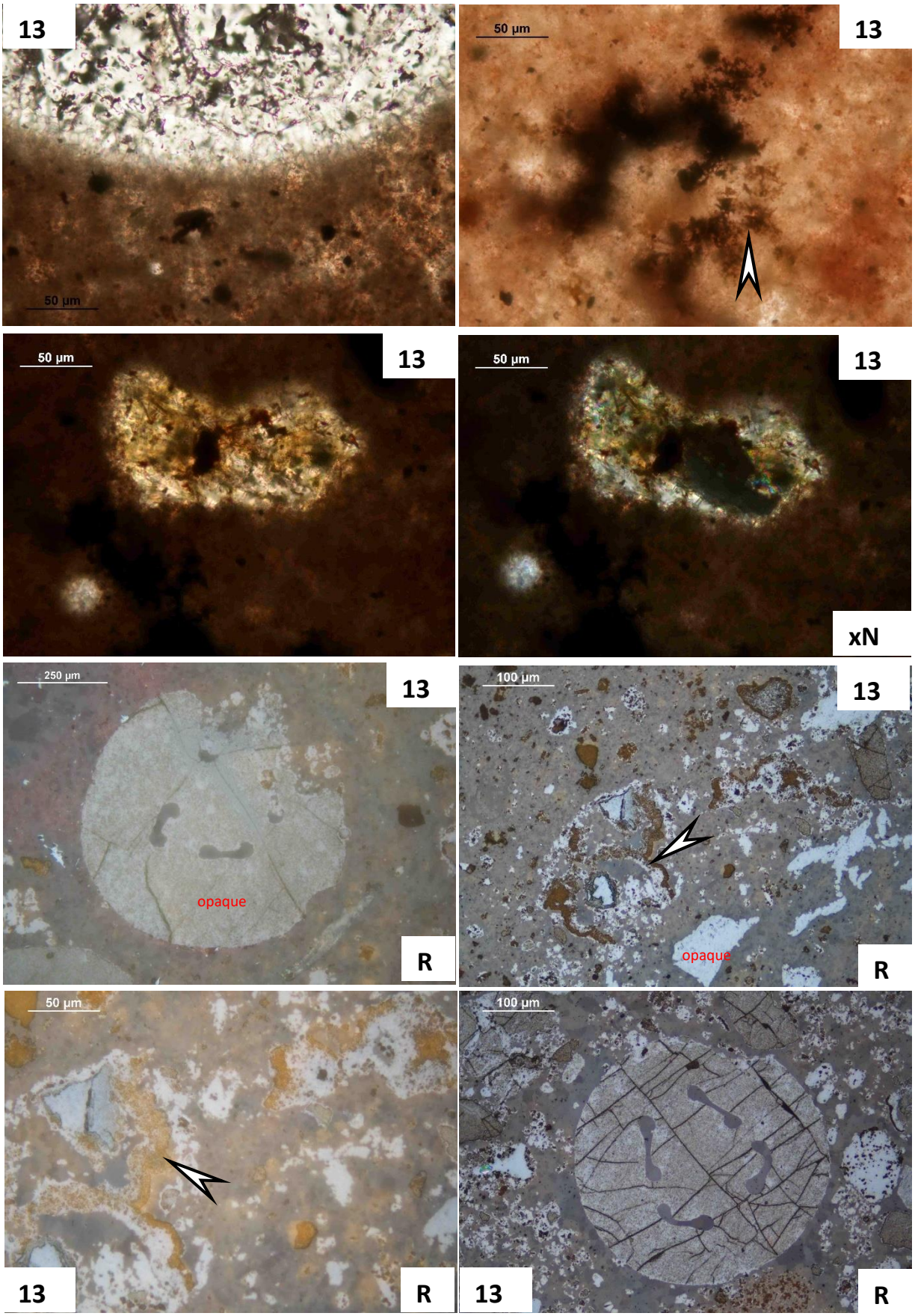
13
50 µm
13
50 µm
50 µm
13
50 µm
13
xN
250 µm
13
opaque
R
100 µm
13
opaque
R
50 µm
13
R
100 µm
13
R

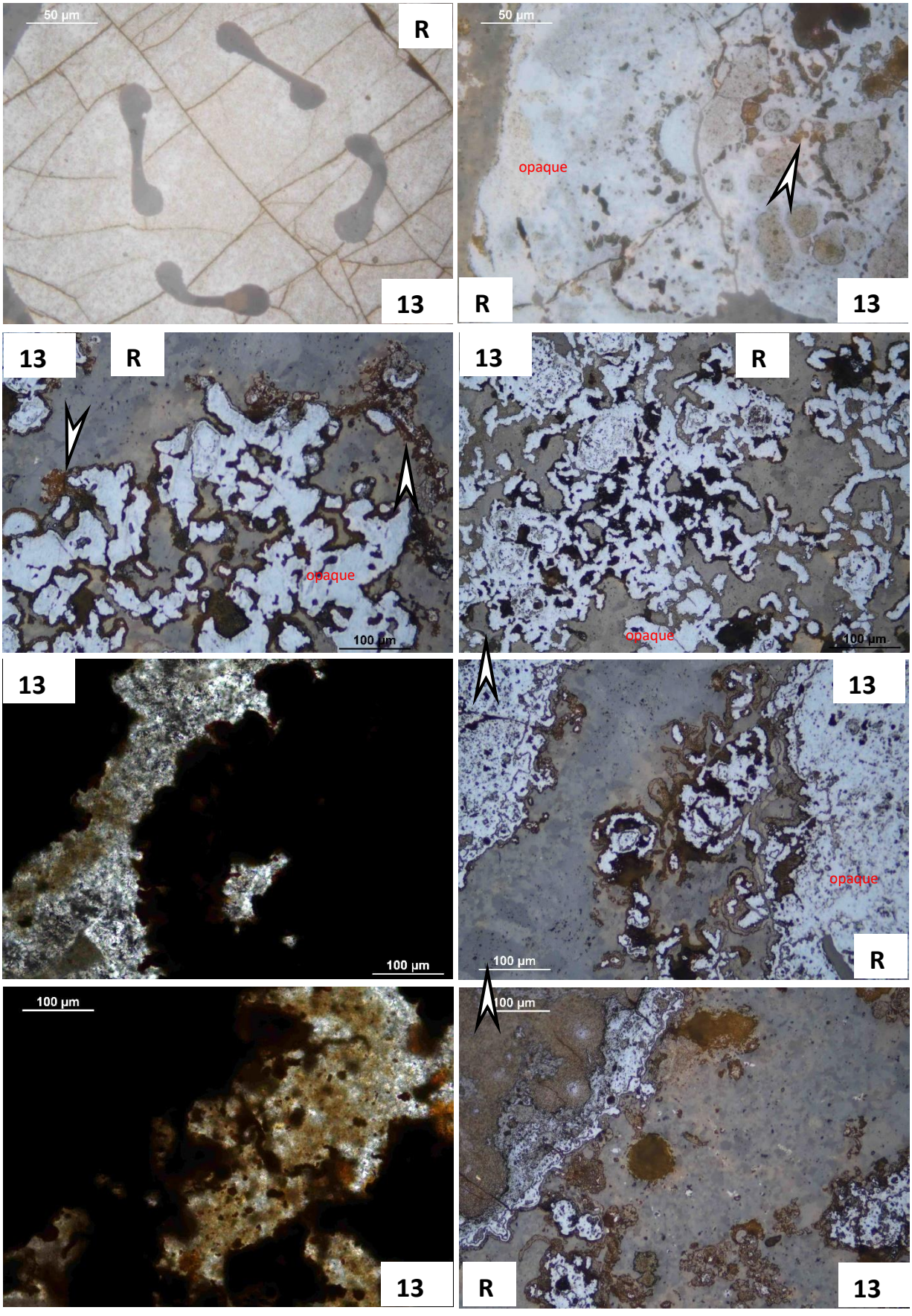
50 µm
R
13
50 µm
opaque
R
13
13
R
opaque
100 µm
13
R
opaque
100 µm
13
100 µm
13
opaque
100 µm
R
100 µm
100 µm
13
R
13

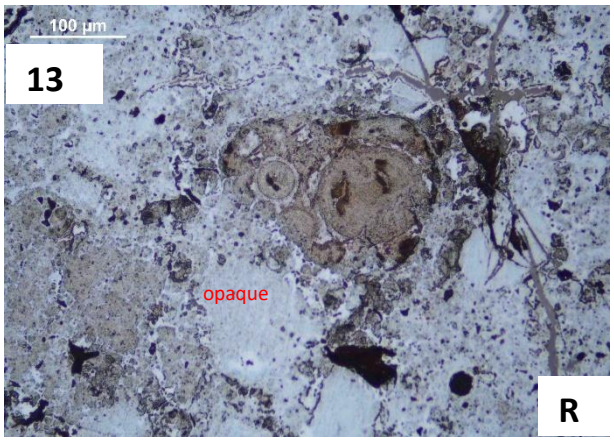
100 µm
13
opaque
R

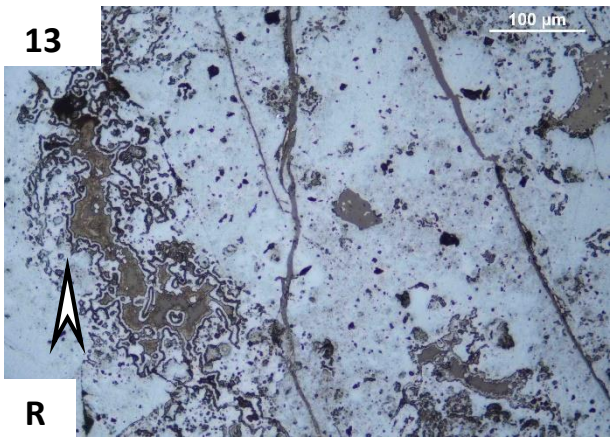
13
100 µm
R

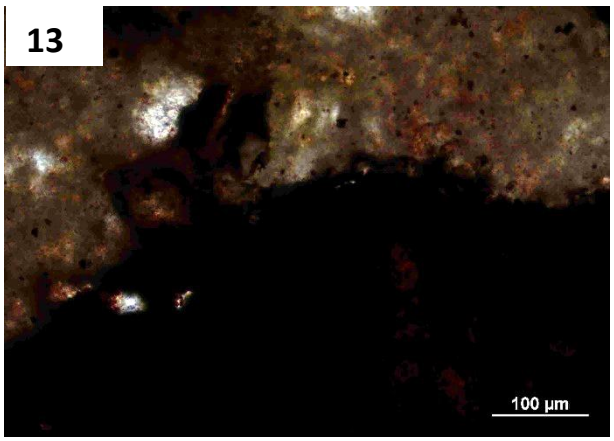
13
100 µm

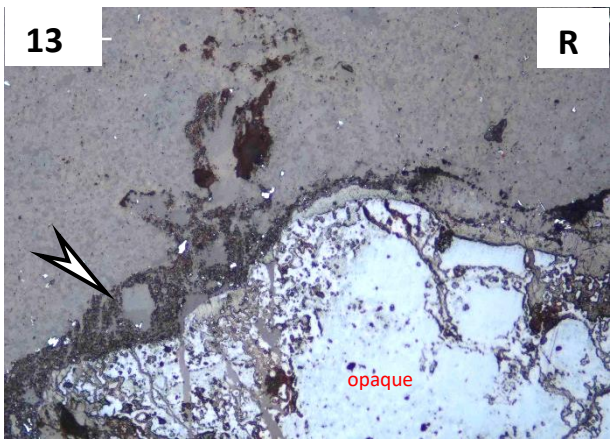
13
R
opaque

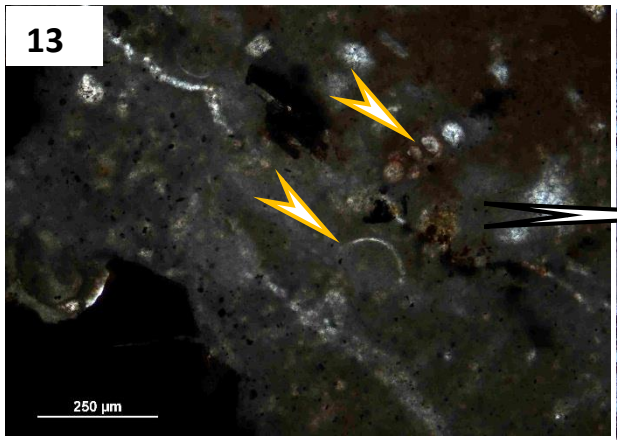
13
250 µm

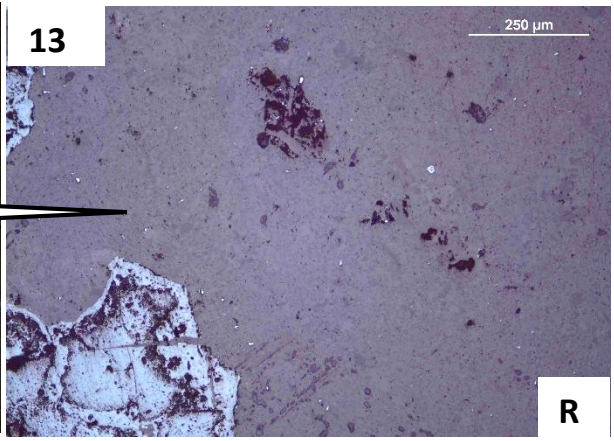
13
250 µm
R

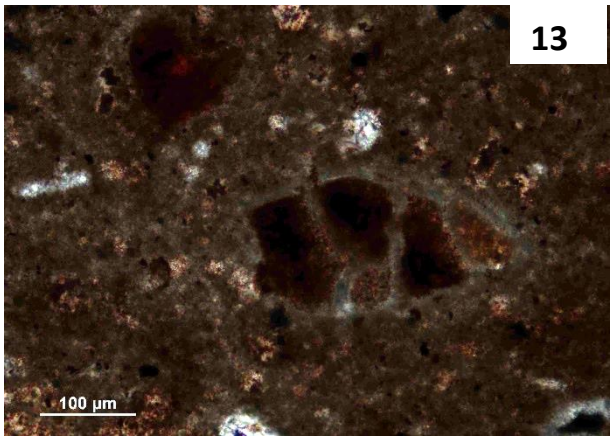
13
100 µm

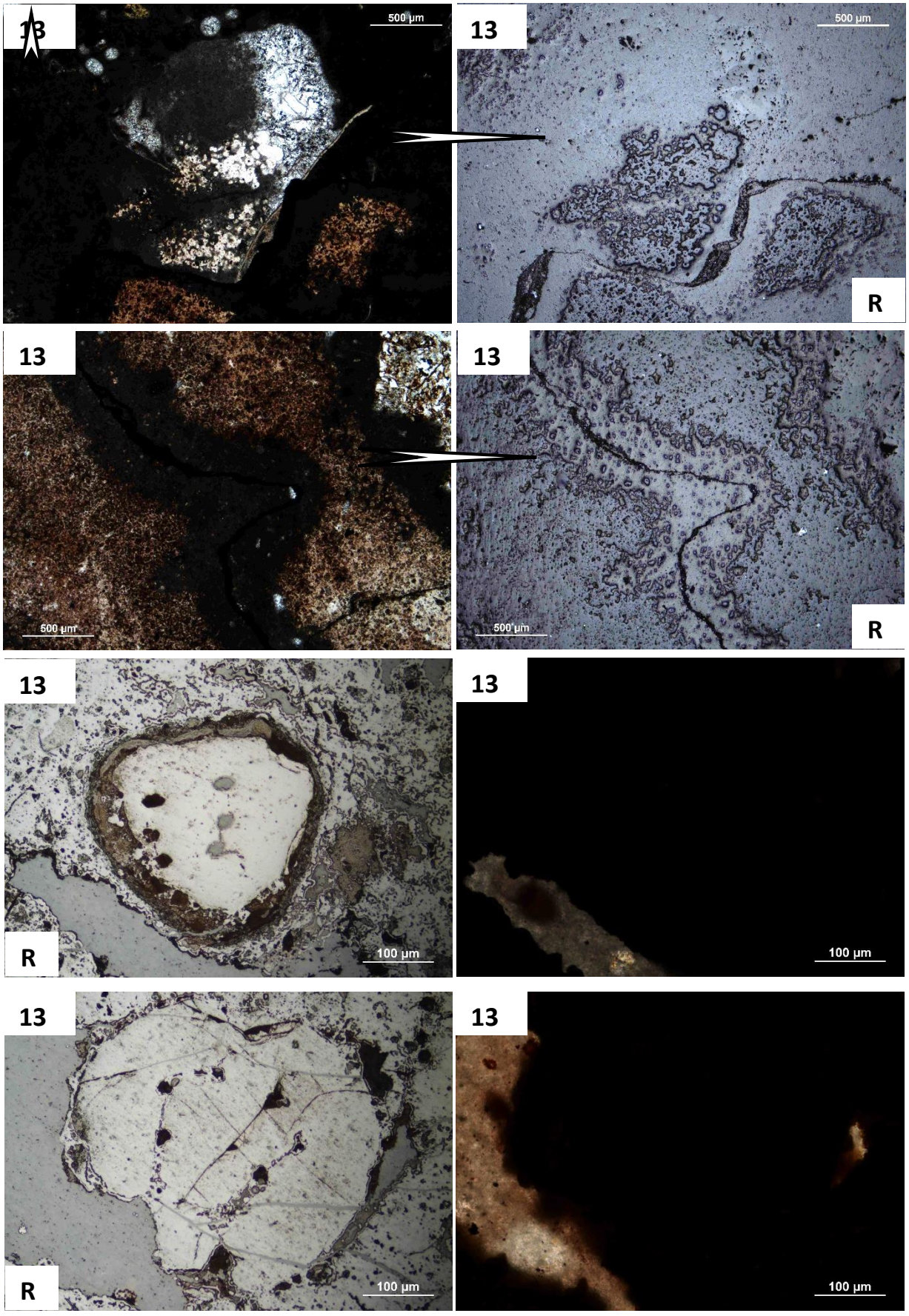
13
500 µm
13
500 µm
R
13
500 µm
13
500 µm
R
13
R
100 µm
13
100 µm
13
R
100 µm
13
100 µm

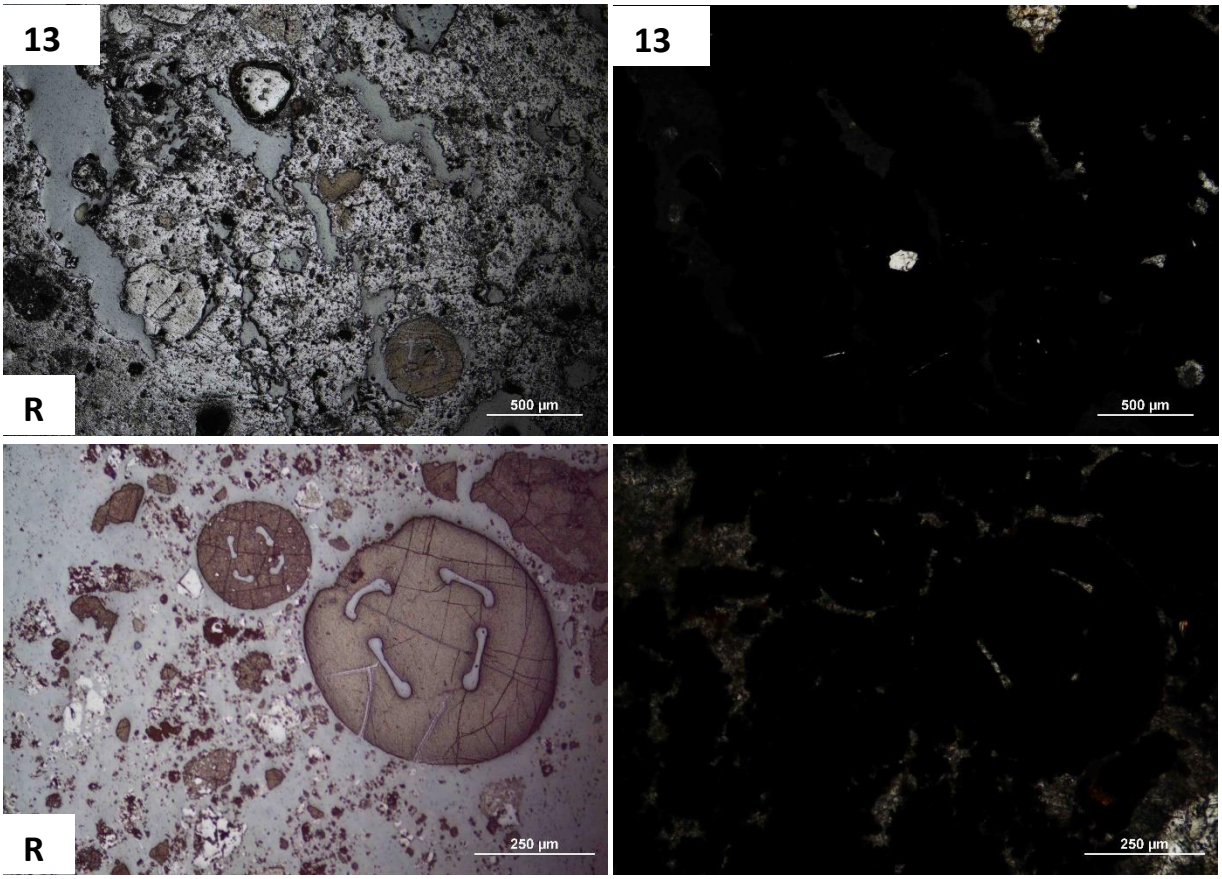

Legend: R-reflective mode; numbers-sample numbers; xN-crossed Nicols
Other microscopy photos were made under transmitted light mode, 1 N

SI Table S1 Mineralogy and organic compounds by Infra-red spectroscopy (FTIR)

Mecsek	**References**	**Sample ID**	**1**							**4**					**9**			**12**			**13**			
Location of measurement			**1**	**2**	**3**	**4**	**5**	**6**	**7**	**1**	**2**	**3a**	**3b**	**4**	**1**	**2**	**3**	**1**	**2**	**3**	**1**	**2**	**3**	**4**
Total No. of spectra→			**8**	**6**	**8**	**11**	**11**	**11**	**9**	**4**	**9**	**6**	**6**	**9**	**9**	**9**	**7**	**7**	**13**	**6**	**5**	**6**	**6**	**6**
Mineral phase		**Wavelength [cm^{-1}]**																						
Carbonates																								
calcite	RRUFF									1			2	4		3	2	5	10		3			1
dolomite	RRUFF														4	1	5							
rhodochrosite	RRUFF	729, 860, 1394											2							2				
kutnohorite	RRUFF	720, 841, 1424						9																
Oxides, hydroxides																								
ferrihydrite	Glotch & Rossman (2009)	692, 878, 3400		1		1	2	2	5	1	3	1			2		4						6	
magnetite	Glotch & Rossman (2009)	580, 1320						9														6		
goethite	Glotch & Rossman (2009)	798, 910, 3400	8					9	5									2	12	4	7	6		5
quartz	Müller et al. (2014)	701, 776, 1059				6				3	3													
Silicates																								
ferrierite	RRUFF	562, 701, 1032vs, 1175 sh, 1625, 3249										4	5	6										
phlogopite	RRUFF	610, 648, 978, 1004								1														
celadonite	Zviagina et al. (2020)	675, 800, 953s, 973s, 1074, 1113, 3641														1								
albite	Müller et al. (2014)	798, 984, 1027sh, 1095, 1103		2	2	3										6								
orthoclase (K-feldspar)	Müller et al. (2014)	717, 1000, 1107sh		3	3	1		9	2						3									

Phosphates																								
apatite	Beasley et al. (2014)	790, 1012, 1093	8		3		9		2								2			2	5			
Sulphates																								
gypsum	RRUFF	610, 681, 1107 vs, 3400, 3526									3				2									
Organic compounds																								
v C=C/C-O	Parikh & Chorover (2006)	1070-1240	3										4					2						
vs CO	Parikh & Chorover (2006)	1360-1450											4	4				2						
d CH2	Parikh & Chorover (2006)	1454-1482	8				11						4	4						6		2		
C-N, CH deformation	Parikh & Chorover (2006)	1526		4				11					4	6										
C-N N-H amide II	Parikh & Chorover (2006)	1540-1550							9	1	9		4					2						
v as COOH	Parikh & Chorover (2006)	1720-29					11	11	9		9		4				7							
C-O	Parikh & Chorover (2006)	1799												6										
CO	Parikh & Chorover (2006)	2343	8		8	11				4	9		6	6	9	9	7	7	13				6	
CO	Parikh & Chorover (2006)	2365	8		8	11				4	9		6	6	9	9	7	7	13				6	
C-H sym. stretch CH2	Parikh & Chorover (2006)	2853					11	11	9				6				7							
C-H asym. stretch CH2	Parikh & Chorover (2006)	2926					11	11	9				6				7							
OH	Madejová & Komádel (2001)	3230-3700								4	9			6					12	4			6	3

References:

Beasley, M. M., Bartelink, E. J., Taylor, L., & Miller, R. M. (2014). Comparison of transmission FTIR, ATR, and DRIFT spectra: implications for assessment of bone bioapatite diagenesis. *Journal of Archaeological Science*, *46*, 16-22.

Glotch, T. D., & Rossman, G. R. (2009). Mid-infrared reflectance spectra and optical constants of six iron oxide/oxyhydroxide phases. *Icarus*, *204*(2), 663-671.

Madejova, J., & Komadel, P. (2001). Baseline studies of the clay minerals society source clays: infrared methods. *Clays and clay minerals*, 49(5), 410-432.

Müller, C. M., Pejcic, B., Esteban, L., Delle Piane, C., Raven, M., & Mizaikoff, B. (2014). Infrared attenuated total reflectance spectroscopy: an innovative strategy for analyzing mineral components in energy relevant systems. *Scientific Reports*, *4*, 6764.

Parikh, S. J., & Chorover, J. (2006). ATR-FTIR spectroscopy reveals bond formation during bacterial adhesion to iron oxide. *Langmuir*, *22*(20), 8492-8500.

RRUFF Database

Zviagina, B. B., Drits, V. A., & Dorzhieva, O. V. (2020). Distinguishing Features and Identification Criteria for K-Dioctahedral 1M Micas (Illite-Aluminoceladonite and Illite-Glauconite-Celadonite Series) from Middle-Infrared Spectroscopy Data. *Minerals*, 10(2), 153.

SI Figure S3 Representative FTIR measurements on sample 1

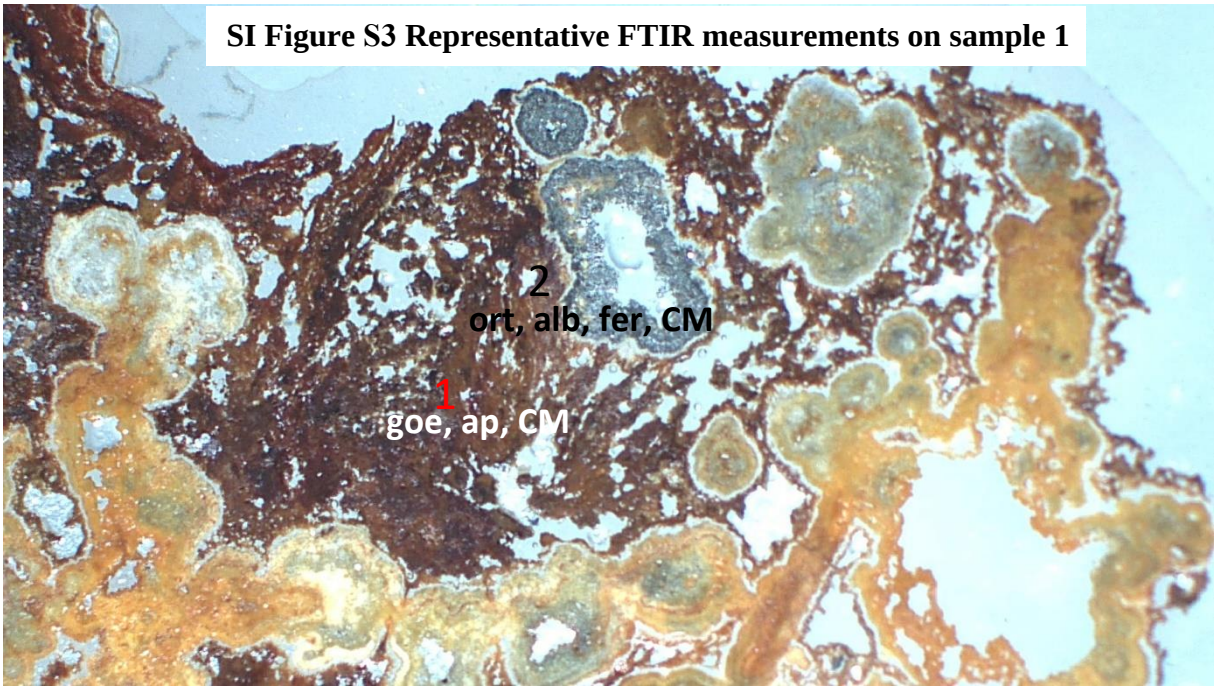

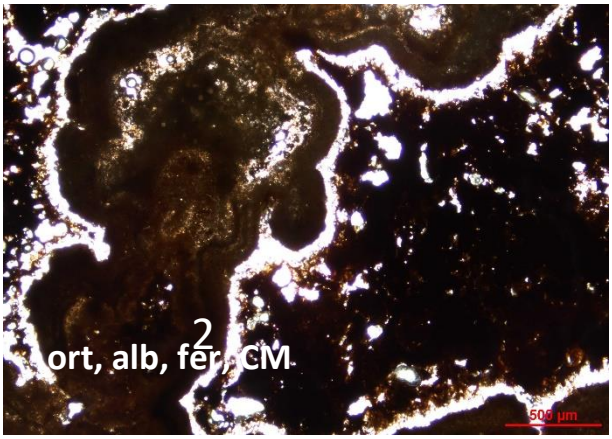

Sample 1 – typical mineralized microbial system
Cross cut of hydrothermal, mineralized discharge system
Legend + CM-carbonaceous material
goe-goethite
mag-magnetite
fer-ferrihydrite
ap-apatite
q-quartz
ort-orthoclase
alb-albite
kutn-kutnohorite

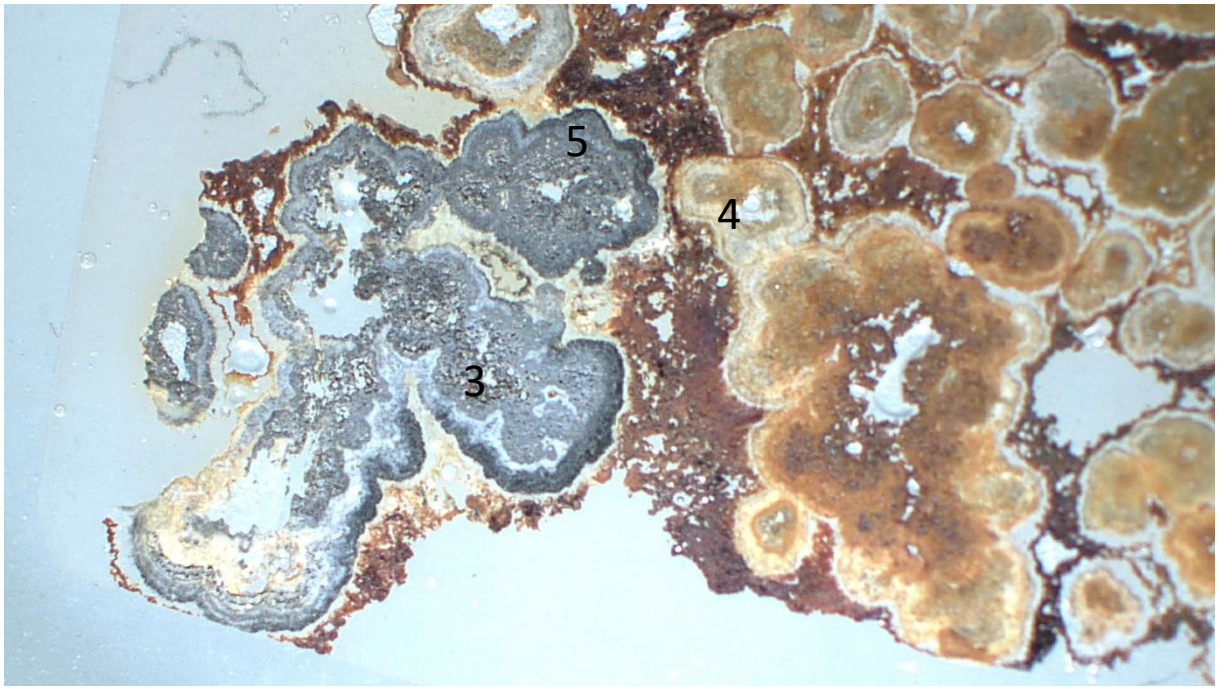

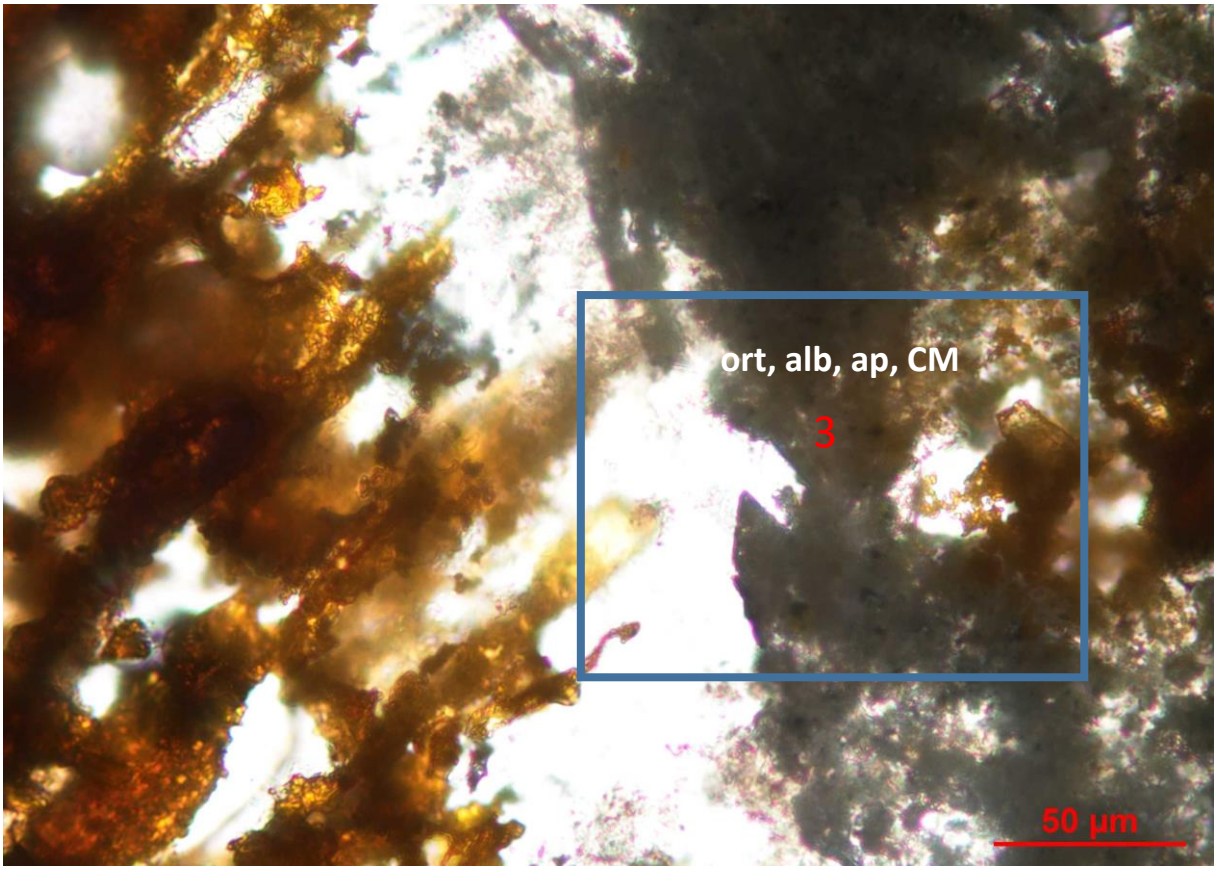
ort, alb, ap, CM
3
50 µm

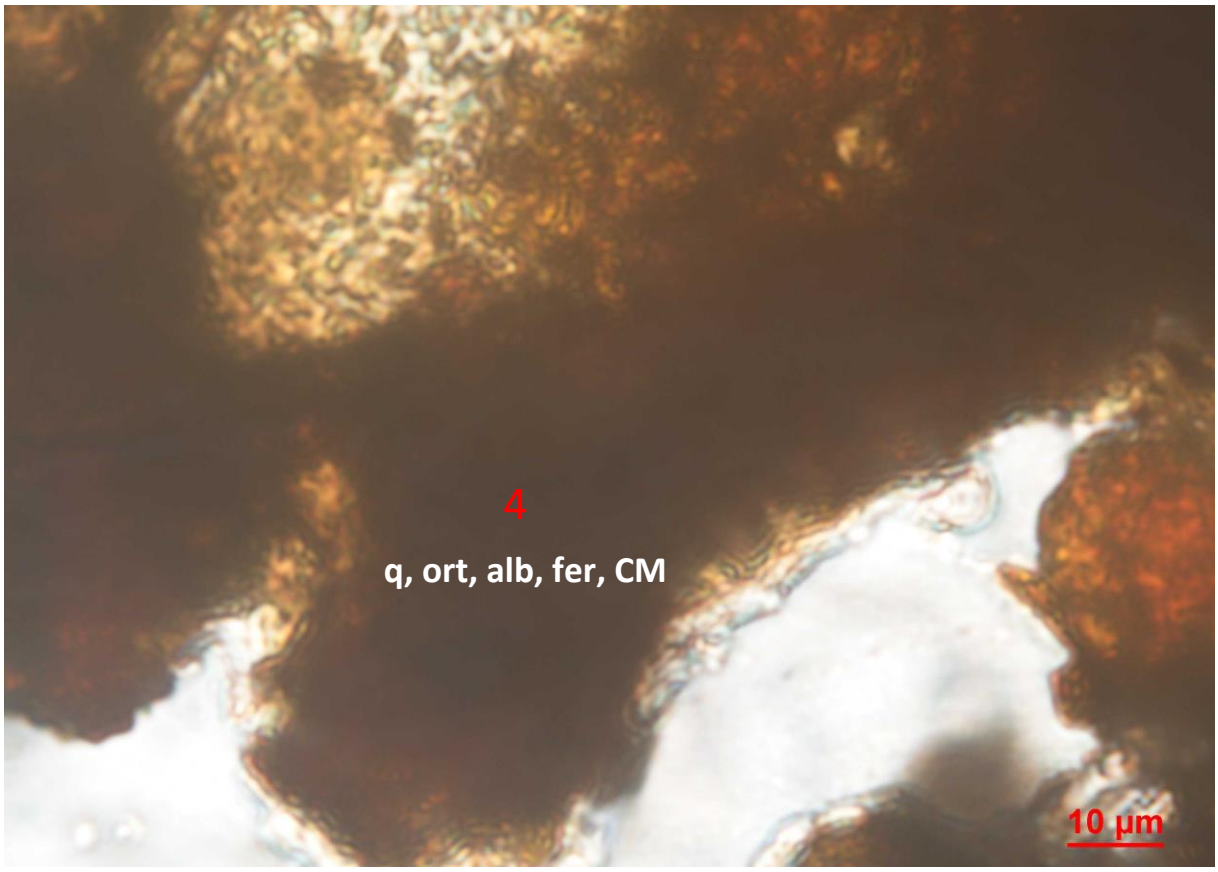
4
q, ort, alb, fer, CM
10 µm

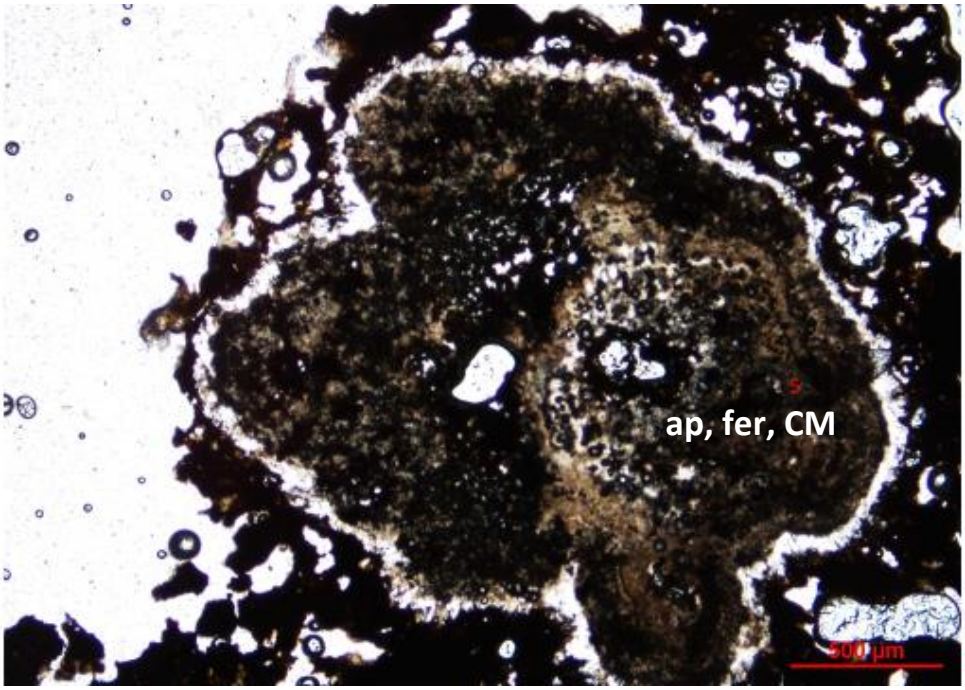
ap, fer, CM
500 µm

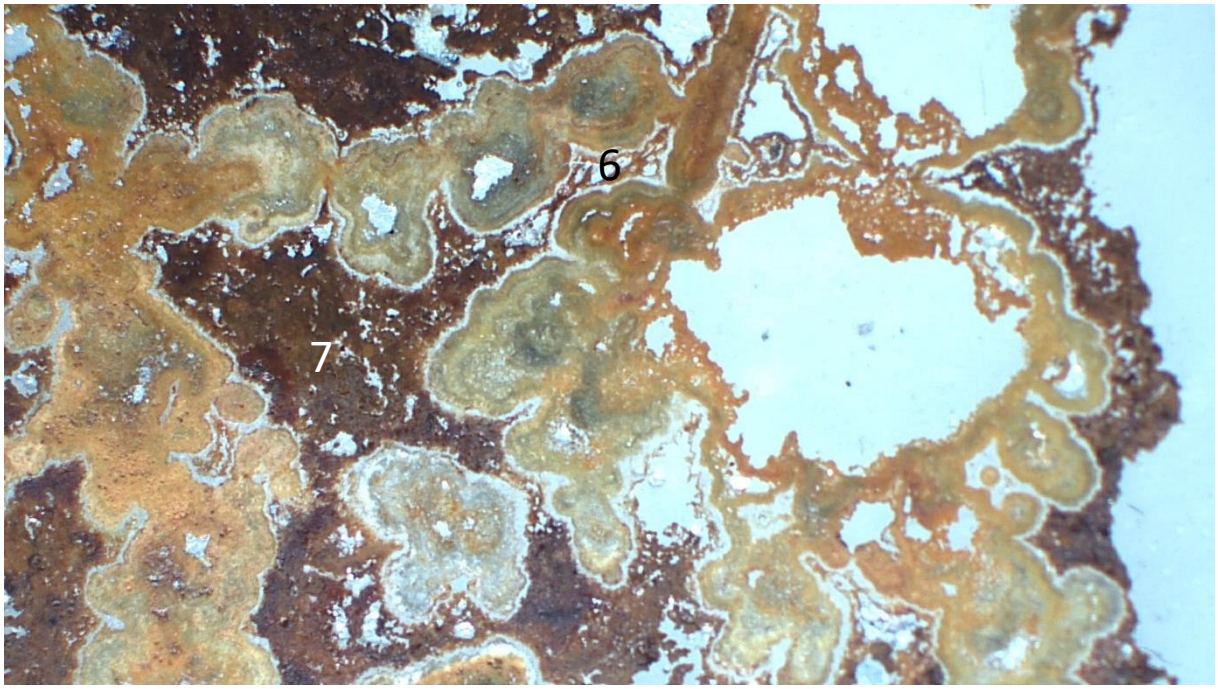
6
7

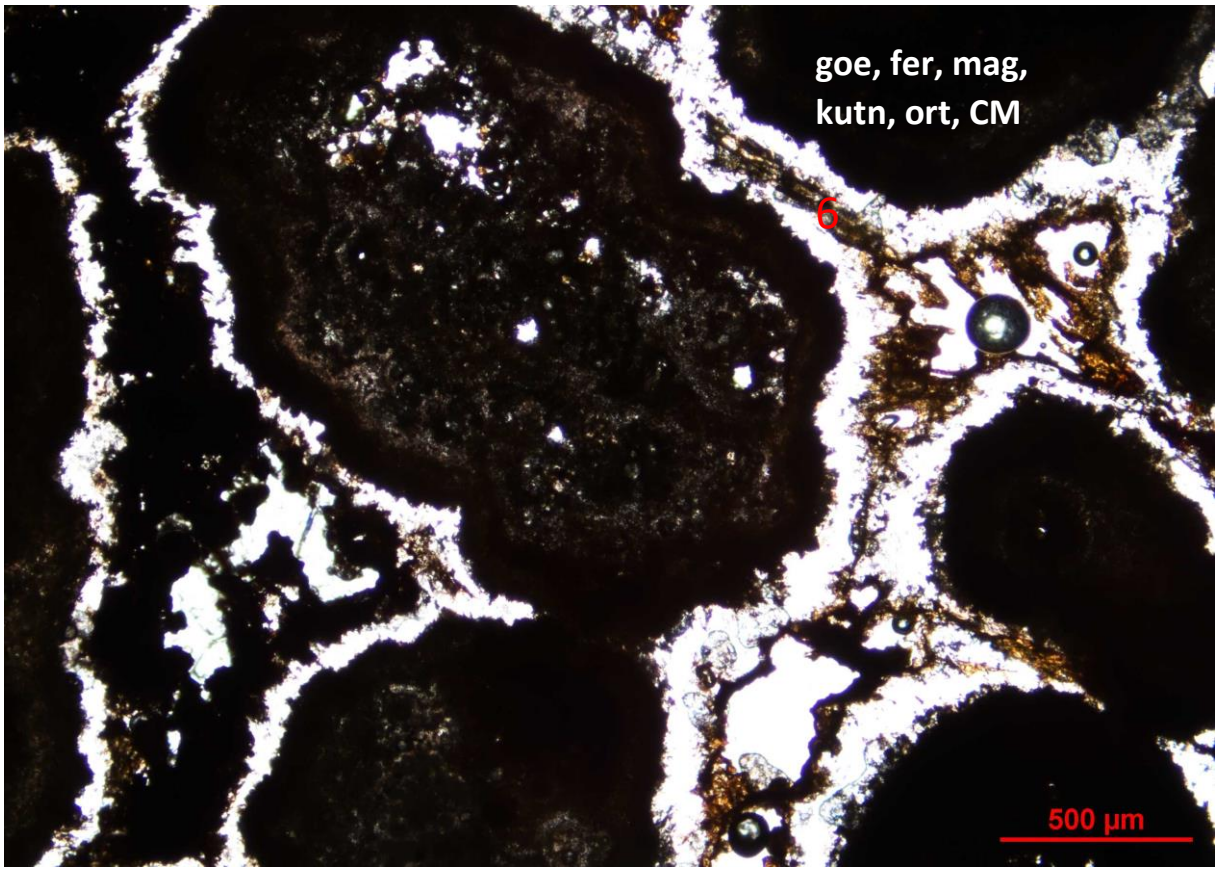
goe, fer, mag,
kutn, ort, CM
6
500 µm

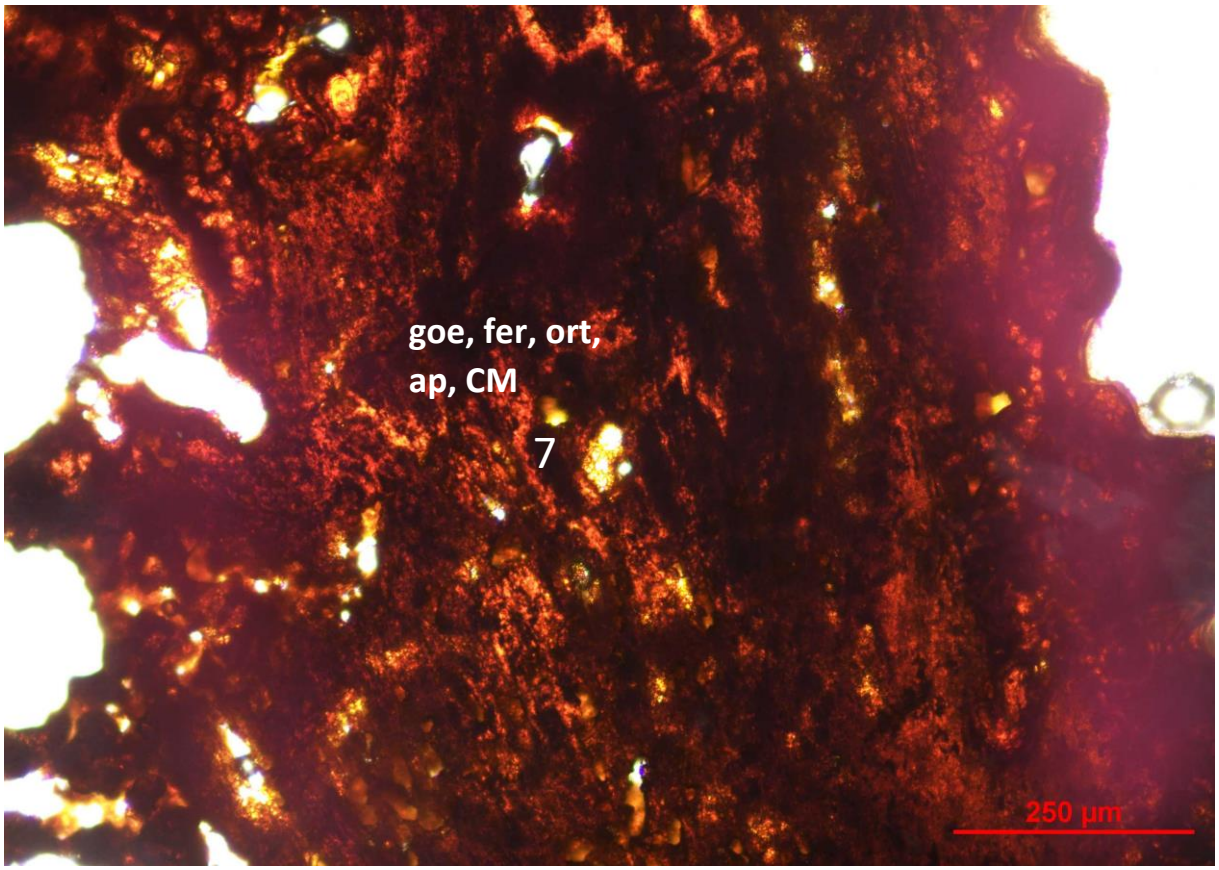
goe, fer, ort,
ap, CM
7
250 µm